# Male mutation rates and the cost of sex for females

**Rosemary J. Redfield**

Department of Zoology, University of British Columbia,
and Program in Evolutionary Biology,
Canadian Institute for Advanced Research,
6270 University Boulevard, Vancouver, British Columbia,
Canada V6T 1Z4

ALTHOUGH **we do not know why sex evolved, the twofold cost of meiosis for females provides a standard against which postulated benefits of sex can be evaluated[1]. The most reliable benefit is sex's ability to reduce the impact of deleterious mutations[2,3]. But deleterious mutations may themselves generate a large and previously overlooked female-specific cost of sex. DNA sequence comparisons have confirmed Haldane's suggestion that most mutations arise in the male germ line[4,5]; recent estimates of $\alpha$, the ratio of male to female mutation rates, are ten, six and two in humans, primates and rodents, respectively[6–8]. Consequently, male gametes may give progeny more mutations than the associated sexual recombination eliminates. Here I describe computer simulations showing that the cost of male mutations can easily exceed the benefits of recombination, causing females to produce fitter progeny by parthenogenesis than by mating. The persistence of sexual reproduction by females thus becomes even more problematic.**

Figure 1 shows three representative selection functions[9], and Fig. 2 some results of simulations using them. All parthenogenetic populations (heavy lines in Fig. 2) reach mutation/selection equilibria at a mean fitness, $W_{eq}$, of $e^{-\mu_f}$, where $\mu_f$ is the genomic mutation rate in females[10,11]. Under independent selection (Fig. 2*a*), when the male genomic mutation rate $\mu_m = \mu_f$ sexual reproduction does not change the population's fitness because, with no epistasis, mutations remain randomly distributed and recombination can have no effect[11,12]. If $\mu_m > \mu_f$, sex drastically reduces fitness; when $\alpha = 2$, 6 and 10, $W_{eq}$ falls from 0.74 to 0.64, 0.35 and 0.19, respectively, precisely the fitnesses predicted by the new mean mutation rates of 0.45, 1.05 and 1.65.

Selection functions incorporating epistasis let us evaluate sex when both recombination and male mutations are affecting mutation load. The moderate epistasis of the quadratic function (Fig. 1*b*) reproduces the observed effects of spontaneous mutations in *Drosophila*[9,13]. Here sexual reproduction increases fitness both when $\alpha = 1$ (to 0.83) and when $\alpha = 2$ (to 0.76), but reduces it if $\alpha = 6$ or 10 (to 0.55 or 0.40). Under truncation selection, accumulating mutations do not change viability until a threshold is reached (here 7) where it falls to zero. This extreme epistasis allows recombination to increase fitness greatly; when $\alpha = 1$ sex raises $W_{eq}$ to 0.96 (Fig. 2*c*). Even here elevated male mutation rates greatly diminish the benefits of sex, eliminating them whenever $\alpha > 5$. (Fitness falls transiently in the first sexual generation because reassortment of the mutations accumulated under parthenogenesis suddenly exposes them to selection.)

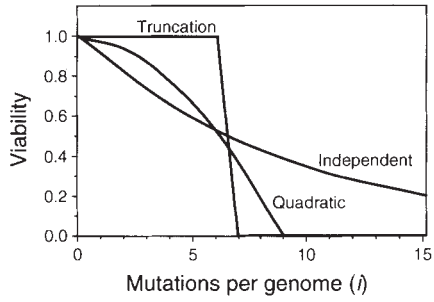


FIG. 1 Selection functions used in the model. *i*, Number of mutations per genome; *v*, viability. Independent selection: $v = 0.9^i$. Quadratic selection: $v = 1 - 0.014i - 0.0112i^2$ (ref. 9). Truncation selection: $v = 1$ for $i < 7$, $v = 0$ for $i \geq 7$.

Figure 3 shows the reverse situation for a wide range of mean mutation rates (quadratic selection, $\alpha = 6$). Each line shows first the equilibrium fitness of a sexual population with a particular mean $\mu$, followed by the change in fitness after parthenogenesis is adopted. The mutation load ($1 - W_{eq}$) is more than halved by parthenogenesis at low mutation rates ($\mu \leq 0.45$), and fitness itself is more than doubled at high rates ($\mu \geq 2.6$). Under parthenogenesis the fitness initially overshoots $W_{eq}$ because of the favourable mutation distribution present at the sexual equilibrium. This also occurs under truncation selection (not shown), and may be evolutionarily significant, as it gives parthenogenesis a short-term benefit even when the equilibrium fitness favours sex.

Because we cannot generalize about the selective consequences of the 'average' mutations assumed by selection functions, I have

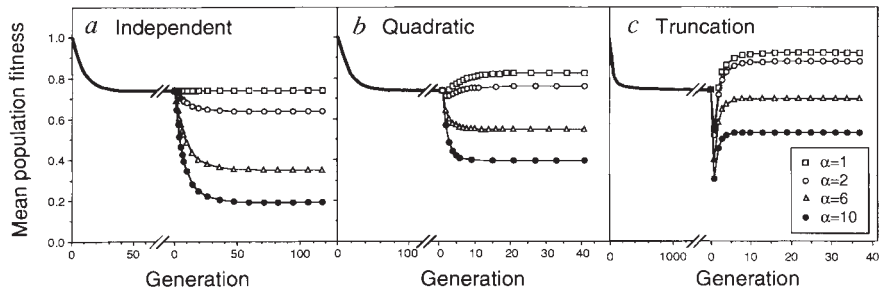


FIG. 2 Mean fitnesses of parthenogenetic and sexual populations under different selection functions and mutation rates. Heavy lines, parthenogenetic populations ($\mu_f = 0.3$) approaching equilibrium. Light lines, sexual populations derived from the asexual populations. *a*, Independent selection; *b*, quadratic selection; *c*, truncation selection. Squares, $\alpha = 1$; empty circles, $\alpha = 2$; triangles, $\alpha = 6$; filled circles, $\alpha = 10$.

METHODS. The model compares parthenogenesis and sexual reproduction by deterministically simulating large populations undergoing repeated generations of viability selection (and reproduction), deleterious germ-line mutation and, where appropriate, sexual recombination by meiosis and gamete fusion. Populations are characterized by their distribution of mutations and by the associated mean fitness *W* (the fraction of the population that will survive the next round of selection against these mutations). Each simulation is continued until the population reaches an equilibrium where mutagenesis is exactly balanced by selection. The simulation is written in ThinkPascal, and run on a Macintosh LCIII. Populations are described by their mutation distributions. The relative frequencies of individuals with different numbers of mutations after selection, male and female germ-line mutagenesis, and recombination are given by the mutation distributions **S**, $\mathbf{M_m}$ or $\mathbf{M_f}$, and **R**. The *i*th term of each distribution gives the frequency of individuals with *i* mutations (*i* ranges from 0 to $i_{max}$). The value of $i_{max}$ was varied between 15 and 50 to minimize runtime while keeping matrix truncation errors below $10^{-7}$. All mutations are unlinked and equally deleterious. Selection: Mutations are co-dominant. Selection functions are described in Fig. 1. Reproduction occurs by normalization of **S**. Mutagenesis: The probability that the male or female acquires *i* new mutations is a Poisson distribution with mean $\mu_m$ or $\mu_f$ Recombination: Mutation distributions in male and female gametes ($\mathbf{G_m}$ and $\mathbf{G_f}$) are calculated from $\mathbf{M_m}$ and $\mathbf{M_f}$. The progeny distribution **R** is then the product of the gamete distributions. Mating is thus random and there is no linkage. Validation of the model: The model was shown to give the expected results under conditions where $W_{eq}$ is known from analytical results: (1) under parthenogenesis: $W_{eq} = e^{-\mu_f}$; (2) under independent selection: $W_{eq} = e^{-\mu}$, where $\mu = \mu_f(1 + \alpha)/2$; (3) using the selection function described by Charlesworth ($v = e^{-ai - bi^2}$), for which $W_{eq}$ has been determined by analytical approximation[3].

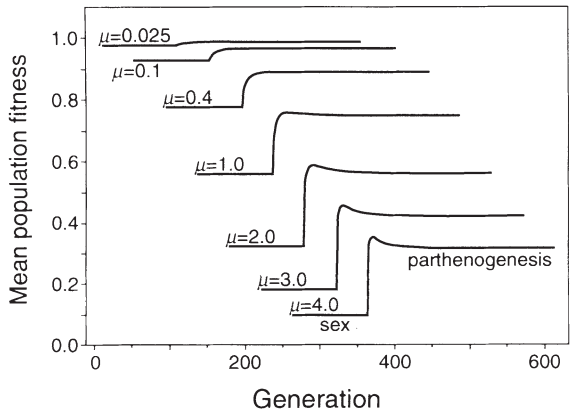


FIG. 3 Mean fitnesses of populations switching from sexual reproduction to parthenogenesis. Mean mutation rate is indicated to the left of each line. Selection is quadratic and $\alpha = 6$. Each population begins at its sexual equilibrium. For clarity, lines are shown staggered by 40 generations.

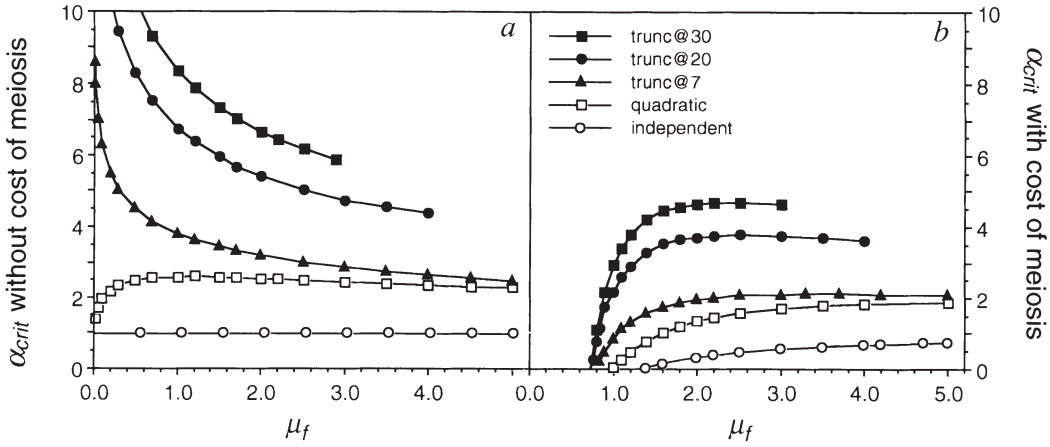


FIG. 4 Critical values of $\alpha$, at which sexual and parthenogenetic reproduction give the same equilibrium population fitness. Selection functions: empty circles, independent; empty squares, quadratic; filled triangles, truncation at 7; filled circles, truncation at 20; filled squares, truncation at 30. *a*, Fitnesses neglect the twofold cost of meiosis for females. *b*, Fitnesses corrected for the twofold cost of meiosis.

examined fitness under a range of conditions. The truncation and independent functions were chosen to represent absolute and no epistasis, respectively, with selection intensities equivalent to that of the biologically based quadratic function. Because most real mutations probably have very minor effects on fitness, I have also tested truncation functions with thresholds of 20 and 30. Figure 4*a* summarizes the results for all these functions by comparing, for different mutation rates, values of $\alpha$ at which parthenogenesis and sex give the same equilibrium fitness ($\alpha_{crit}$). Under independent selection $\alpha_{crit} = 1$. With quadratic selection, parthenogenesis is favoured when $\alpha > 2.5$, unless the mutation rate is very low. Truncation selection gives similar $\alpha_{crit}$ at high mutation rates, but at low rates sexual females can tolerate higher values of $\alpha$.

In many sexual species females do all of the work of reproduction but can pass on only half of their genes. The analysis in Fig. 4*b* incorporates this cost by requiring that each sexual population's fitness be twice that of the corresponding parthenogenetic population. This precludes any net advantage of sex if $\mu < 0.7$, or under independent selection (unless $\alpha < 1$). Increasing the epistatic component of selection increases the benefits of recombination and thus the tolerance of male mutations, but under the conditions examined $\alpha_{crit}$ never exceeds 5 and shows little dependence on mutation rates above $\mu_f = 2$. However, $\alpha_{crit}$ may be larger under selection functions, allowing still more mutations to accumulate. Stochastic effects, known to increase the costs of deleterious mutations[14], could also increase (or decrease) tolerance of elevated male mutation rates.

Elevated germ-line mutation rates may be an inevitable consequence of producing large numbers of gametes, male or female. Chang *et al.*[8] found a correspondence between male and female point mutation rates and the number of cell divisions in the corresponding germ lines, supporting the hypothesis that these mutations arise during DNA replication. This predicts that $\alpha$ will be highest in species where males produce far more gametes than do females, for example, wind-pollinated plants and aquatic animals with external fertilization.

Given that even small increases in mutation rates significantly decrease fitness, how might parents reduce the number of new mutations in their progeny? The obvious solution, increasing the fidelity of germ-line-specific DNA polymerases and DNA repair pathways, will slow cell division and may decrease male fecundity. Females with physiological commitments preventing a switch to parthenogenesis (such as mammals) might reduce the contribution from male mutations by mating with the youngest males available, as their gametes will have undergone the fewest rounds of DNA replication. Although each generation's new mutations make only a minor contribution to total mutation load, the cumulative effect of reducing them can be substantial.

Kondrashov has shown that in large populations recombination of deleterious mutations can overcome the twofold cost of sex for females only if mutation rates are high ($\mu > 1$) and selection incorporates substantial epistasis[2,15,16]. Unfortunately, the simulations described above suggest that, even when these conditions are met, females will be selected to give up sex entirely if male mutation rates are excessively high. That they have not done so leaves us in a quandary. If male mutations are not the major cost to females that this model suggests, it should be because deleterious mutations are less important than we have thought. But what could then pay the twofold cost of meiosis for females? One possibility is the antagonistic selection imposed by coevolving parasites, which, in combination with selection against deleterious mutations, can greatly increase the benefits of sex[17,18]. To clarify these issues we urgently need more data about the rates and selective consequences of real mutations in real populations. □

Received 17 September 1993; 16 March 1994.

1. Maynard Smith, J. *The Evolution of Sex* (Cambridge Univ. Press, Cambridge, 1978).
2. Kondrashov, A. S. *Nature* **336,** 435–440 (1988).
3. Charlesworth, B. *Genet. Res., Camb.* **55,** 199–221 (1990).
4. Haldane, J. B. S. *Ann. Eugen.* **13,** 262–271 (1947).
5. Miyata, T., Hayashida, H., Kuma, K., Mitsuyasu, K. & Yasunaga, T. *Cold Spring Harb. Symp. quant. Biol.* **52,** 863–867 (1987).
6. Montandon, A. J. *et al. Hum. Genet.* **89,** 319–322 (1992).

7. Shimmin, L. C., Chang, B. H.-J. & Li, W.-H. *Nature* **362,** 745–747 (1993).
8. Chang, B. H.-J., Shimmin, L., Shyue, S.-K., Hewett-Emmett, D. & Li, W.-H. *Proc. natn. Acad. Sci. U.S.A.* **91,** 827–831 (1994).
9. Crow, J. F. in *Mathematical Topics in Population Genetics* (ed. Kojima, K.) 128–177 (Springer, Berlin, 1970).
10. Haldane, J. B. S. *Am. Nat.* **71,** 337–349 (1937).
11. Kimura, M. & Maruyama, T. *Genetics* **54,** 1303–1312 (1966).
12. Maynard Smith, J. *Am. Nat.* **102,** 469–473 (1968).
13. Mukai, T. *Genetics* **61,** 749–761 (1969).
14. Muller, H. J. *Mutat. Res.* **1,** 2-9 (1964).
15. Kondrashov, A. S. *Genet. Res., Camb.* **44,** 199–217 (1984).
16. Kondrashov, A. S. & Crow, J. F. *Hum. Mutat.* **2,** 229–234 (1993).
17. Hamilton, W.D., Axelrod, R. & Tanese, R. *Proc. natn. Acad. Sci. U.S.A.* **87,** 3566–3573 (1990).
18. Howard, R. S. & Lively, C. M. *Nature* **367,** 554–557 (1994).

ACKNOWLEDGEMENTS. I thank H. Ochman for pharmacological support, M. McLeod for assistance with programming, and T. Cavalier-Smith, L. Shimmin, J. Berger, B. Charlesworth and especially A. Kondrashov for comments on the manuscript. I thank the Medical Research Council of Canada for financial support.

# Antigen processing and class II MHC peptide-loading compartments in human B-lymphoblastoid cells

**Michele A. West, John M. Lucocq*† & Colin Watts**

Department of Biochemistry, Medical Sciences Institute, University of Dundee, Dundee DD1 4HN, UK
* Department of Anatomy, University of Berne, CH-3000 Berne, Switzerland

**THE peptide/class II major histocompatibility complex (MHC) complexes recognized by $CD4^+$ T cells have been characterized at the structural[1] and biochemical[2–4] levels and studies on the transport and maturation of class II MHC indicate that specialized sites may be involved in peptide acquisition[5–11]. Here we report the characterization of the compartments involved in antigen processing and class II MHC loading relative to distinct functional domains of the endocytic pathway in antigen-specific human B lymphocytes[12–14]. Peroxidase-mediated crosslinking analysis[15] in intact cells demonstrates that peptide loading of class II MHC takes place in a compartment accessible to membrane immunoglobulin but not to transferrin receptors, although processing may be initiated within the latter domain. The density of membrane vesicles carrying newly assembled class II MHC complexes was distinct from early and late endosomes and dense lysosomes. Endocytosed antigen–gold complexes enter a class II MHC-rich compartment morphologically very similar to that described previously[9] and within the time frame of biochemically detectable peptide loading.**

Tetanus-toxin-specific human B-lymphoblastoid cells were pre-loaded with $^{125}$I-labelled antigen at 0 °C, washed and incubated at 37 °C[13,14]. After 30 min, sodium dodecyl sulphate (SDS)-stable class II $\alpha\beta$ dimers become labelled with processed tetanus toxin peptides (ref. 16 and Fig. 1*a*). In this system, surface expression of antigen-loaded class II MHC, detected either by T-cell assay[17] or by direct surface biotinylation (S. Moore and C.W., unpublished results), occurs 45–60 min after antigen uptake, that is ~15–30 min after their intracellular assembly. To analyse the intracellular location of newly assembled complexes, we first used a non-disruptive method of cellular compartmental analysis. Endocytosed horseradish peroxidase (HRP) or HRP-conjugates generate a dense crosslinked polymer on incubation with 3,3′-diaminobenzidine (DAB) and $H_2O_2$. Only proteins within the compartments carrying the HRP probe are polymerized and rendered detergent-insoluble[15,18]. Thus, different peroxidase conjugates (such as transferrin–HRP (Tf-HRP) or antigen–HRP) can be used to probe the location, in intact cells, of distinct biochemical intermediates in antigen processing. Control experiments demonstrated very efficient $H_2O_2$-dependent polymerization (>90%) of the Tf-HRP probe and co-internalized transferrin, which fail to enter the stacking gel (Fig. 1*b*). To analyse the location of newly assembled intracellular peptide/class II MHC complexes, antigen-specific B-lymphoblastoid cells were pre-loaded with $^{125}$I-labelled antigen at 0 °C and chased at 37 °C to allow antigen uptake and processing. Tf-HRP was included during the last 30 min. Cell aliquots were incubated with DAB at 0 °C in the presence or absence of $H_2O_2$, then class II MHC molecules were immunoprecipitated and analysed by SDS–PAGE. Class II $\alpha\beta$ dimers, labelled with processed antigen-derived peptides after 30 or 60 min, escaped crosslinking by Tf-HRP (Fig. 1*c*, lanes 1 and 2, 3 and 4). In contrast, when antigen–HRP replaced Tf-HRP during the chase, intracellular class II complexes were now efficiently crosslinked and therefore not immunoprecipitated (>60%; Fig. 1*c*, compare lanes 7 and 8). (A cohort of unoccupied membrane immunoglobulin recycles to the cell surface under these conditions[14] allowing virtually simultaneous uptake of both radiolabelled and peroxidase-conjugated antigen.) Mixing experiments established that crosslinking of class II $\alpha\beta$ dimers was occurring within intact cells (lanes 9 and 10; see legend) and was not simply due to greater uptake of this conjugate compared to the Tf-HRP conjugate (not shown).

In the same cells we also assessed the distribution of a set of non-MHC-associated clonotypic antigen fragments ($M_r$ range 3K–16K) that remain bound to immunoglobulin[13]. In contrast to peptide-loaded class II MHC molecules, a significant proportion (40–60%) of these antigen fragments were consistently crosslinked by Tf-HRP (Fig. 1*c*, lanes 13 and 14). Control experiments established that this was mediated by specific uptake of Tf-HRP and was not due to missorting of the Tf-HRP conjugate (see legend). When the antigen–HRP probe was used, almost complete (80–90%) crosslinking of these fragments occurred (Fig. 1*c* lanes 15 and 16).

Taken together, these experiments indicate that newly assembled peptide/class II MHC complexes reside in a compartment accessible to antigen through membrane immunoglobulin-driven uptake, but not to endocytosed transferrin receptors. Transferrin receptor-positive early and late endosomes[19,20] support some antigen processing but are unlikely to be major stations of class II MHC assembly.

To analyse further the compartment containing loaded class II/peptide complexes we fractionated post-nuclear supernatants from antigen-pulsed B cells on 27% Percoll gradients[14]. Markers of plasma membrane, early/late endosomes and late endosomes/pre-lysosomes (membrane IgG, internal transferrin receptor and CI-mannose-6-phosphate receptor, respectively) migrated in the low-density fractions (peak density, 1.04 g ml$^{-1}$), whereas the lysosomal marker $\beta$-hexosaminidase peaked at 1.088 g ml$^{-1}$ (Fig. 2*a*). During uptake and processing, the $^{125}$I-label (intact antigen and immunoglobulin-bound fragments) slowly shifted from the low-density plasma membrane/endosome fractions to populate intermediate-density membranes between 30 and 60 min, then denser fractions after longer chase times (Fig. 2*b* and ref. 14). Class II MHC molecules were immunoprecipitated from pooled pairs of gradient fractions and analysed without boiling to preserve SDS-stable peptide/class II MHC complexes[16]. Most of the earliest detectable class II/peptide complexes were found in intermediate density fractions 17–20 ($\rho = \sim 1.06$ g ml$^{-1}$) distinct from the plasma membrane/endosome fractions (7–12) and the peak of lysosomal $\beta$-hexosaminidase (fractions 23/24) (Fig. 2*c*, *d*). As peptide-labelled $\alpha\beta$ complexes accumulated (5.6-fold increase between 30 and 60 min; see Fig. 1*a*), they appeared in the plasma membrane fractions as expected, but also in progressively denser fractions; ~1.07 g ml$^{-1}$ (60 min), 1.088 g ml$^{-1}$ (360 min). Because surface expression is achieved well before comigration with the $\beta$-hexos-

† Present address: Department of Anatomy and Physiology, Medical Sciences Institute, University of Dundee, Dundee DD1 4HN, UK.